Journal of the Optical Society of America B
OPTICAL PHYSICS

Controlling the null photonic gap and zero refractive index in photonic superlattices with temperature-controllable-refractive-index materials

YE WU,[1] PENGFEI OU,[2] LING ZHANG,[3,*] YINGCHENG LIN,[3,4,5] AND JIQUAN YANG[1,6]

[1]School of Electrical and Automation Engineering, Jiangsu Key Laboratory of 3D Printing Equipment and Manufacturing, Nanjing Normal University, Nanjing, 210046, China
[2]Department of Mining and Materials Engineering, McGill University, Montreal, Quebec H3A 0C5, Canada
[3]College of Microelectronics and Communication Engineering, Chongqing University, Chongqing, 400044, China
[4]Key Laboratory of Dependable Service Computing in Cyber Physical Society of Ministry of Education, Chongqing University, Chongqing, 400044, China
[5]e-mail: linyc@cqu.edu.cn
[6]e-mail: yangjiquan@njnu.edu.cn
*Corresponding author: zhangling1993@cqu.edu.cn

Received 18 December 2019; revised 28 January 2020; accepted 10 February 2020; posted 10 February 2020 (Doc. ID 384702); published 10 March 2020

Temperature-adjustable optical properties of two types of one-dimensional photonic superlattices made from lithium niobate or liquid crystal are theoretically investigated. The control of band structures and density of states is achieved through the temperature with various values of refractive index, layer width, and propagation wavelength. It is presented that a null photonic gap appears at certain temperature points, which are decided by the ratio of layer width and the refractive index. It is shown that the spatial average of the wave vector $\langle k \rangle$ vanishes at a specific temperature as functions of the layer thickness and refractive index. The values of the temperature corresponding to zero-refractive-index (zero-$\langle n \rangle$) are demonstrated to be suppressed when the refractive index or the ratio of the layer width is enhanced. Null photonic gap and zero-$\langle n \rangle$ can appear simultaneously at certain wavelengths in the range of visible light, which can be modulated by the temperature. This implies the importance of one-dimensional photonic superlattices made from temperature-controllable-refractive-index materials for many important practical applications.

https://doi.org/10.1364/JOSAB.384702

1. INTRODUCTION

A great deal of attention has been paid to the study of temperature-controllable-refractive-index materials [1–14], given that the refractive index is an important parameter in optics. The properties associated with the tunable refractive index presented in these materials are attractive for making adjustable-focus lenses, prism gratings, spatial light modulators, and other adaptive photonic devices [15–25].

Artificial optical waveguides have been an interesting research subject if one considers their properties and potential technological applications in a wide range of optical devices, including a zero-refractive-index (zero-$\langle n \rangle$) gap [15], discrete and photon tunneling modes [16], spontaneous photon production [17], dipole-dipole interactions [18], and large optical nonlinearity [19]. All these studies are based on an environment with fixed temperature and are focused on the use of left-handed materials whose physical parameters ε and μ are very dispersive. We believe that these waveguide structures, although of great scientific and technological interest on their own, do not provide the flexibility in using tunable waveguides.

A question may arise: can we introduce more dispersive values of the refractive index through the modulation of the temperature and therefore modify the band structures? After all, the manipulation of the temperature is seemingly convenient to be done in a modern lab considering the easy access of commercial furnaces and refrigerators.

Let us speculate: when the temperature is changing, there may be a critical value of the refractive index existing that can make the corresponding photonic structure resonant. At this critical refractive index associated with the temperature, the interaction between radiation field and photonic structure may be strong enough, and the wave inside the waveguide could

correspond to a coupled mode contributing the whole material system. Such a coupling may impact the propagation of the radiation field in a very profound manner and give rise to novel effects.

For further practical applications of superlattices made from temperature-controllable-refractive-index materials, it is important to know how the band structures, density of states, and null photonic gap vary according to temperature. It is also important to understand how varying geometrical parameters of the superlattices can affect the photonic properties with the combination of temperature.

Another problem that captivates our research interest is controlling the zero-$\langle n\rangle$ [26–30]. Since the beginning of optical material study, the optical properties of media with a refractive index near zero have attracted the interest of the scientific community. It can be noted that $\Delta n = \Delta\varepsilon/(2\varepsilon^{0.5})$, [30] where Δn is the change of the refractive index, $\Delta\varepsilon$ is the change of permittivity, and ε is the permittivity. One may find out when the permittivity is approaching zero that tremendous variation of the refractive index can appear, suggesting that the materials at that near-zero-$\langle n\rangle$ point should show strong nonlinear optical properties. This is the reason why zero-$\langle n\rangle$ is so important. In a material system possessing a temperature-controllable refractive index, we are curious about how zero-$\langle n\rangle$ can be developed along with adjusting the temperature. We are urged to find out at what critical temperature point zero-$\langle n\rangle$ can arise and how this critical temperature would be impacted.

This motivates us to study how the temperature affects the band structures, density of the states, null photonic gap and zero-$\langle n\rangle$ in photonic superlattices, which, up to now, have not been addressed in previous studies to our knowledge.

Here two material systems corresponding to two types of temperature-controllable-refractive-index materials (i.e. lithium niobate and liquid crystal) are studied. A detailed study of the temperature-directed band structures and density of the states, along with the change of refractive index, material width, and propagation wavelength is presented. The values of temperature corresponding to the null gap can be adjusted by the layer width ratio and refractive index.

The temperature condition when zero-$\langle n\rangle$ appears is investigated. The propagation wavelength associated with concurrence of the zero-$\langle n\rangle$ and null gap is found to be controllable by the temperature.

The paper is organized as follows. In Section 2, the theoretical approach is detailed. Section 3 is concerned with results and discussion. Finally, our conclusions are provided in Section 4.

2. THEORETICAL MODEL

A. Theoretical Model of Dispersion Equation in a 1D Photonic Superlattice

A 1D photonic superlattice in the z direction, i.e., a periodic photonic heterostructure composed of alternating layers of different layer materials, is proposed. The origin is located at the center of a first slab (with dielectric constant ε_1 and magnetic permeability μ_1) of width a_1 with period $a = a_1 + a_2$, where a_2 is the slab width of the second material (with dielectric constant ε_2 and magnetic permeability μ_2). For simplicity, the analysis is restricted to electromagnetic (EM) plane waves. The propagation of EM waves is considered to be along the z axis of the superlattice. Its form is given by

$$\vec{E}(z,t) = E(z)e^{-i\omega t}\hat{x}. \tag{1}$$

By using Maxwell's equations for linear and isotropic media, [31,32] the amplitude $E(z)$ of the electric field can be derived as

$$\frac{d}{dz}\left[\frac{1}{n(z)Z(z)}\frac{dE}{dz}\right] = -\frac{n(z)}{Z(z)}\frac{\omega^2}{c^2}E, \tag{2}$$

where $n(z) = \varepsilon(z)^{1/2}\mu(z)^{1/2}$ and $Z(z) = \mu(z)^{1/2}/\varepsilon(z)^{1/2}$ are the refraction index and impedance with respect to each layer material. Equation (2) can be solved as

$$E(z) = c_1\cos[k(z-z_o) + \frac{c_2}{k}\sin[k(z-z_0)], \tag{3}$$

where z_0 represents the position of an arbitrary point in each layer and $k = \omega n/c$. For simple calculation, a function of

$$\varphi(z) = \begin{bmatrix} E(z) \\ \frac{1}{nZ}\frac{dE}{dz} \end{bmatrix} \tag{4}$$

is introduced. It satisfies

$$\varphi(z) = TT\varphi(z_0), \tag{5}$$

where TT is a 2×2 transfer matrix expressed as

$$TT = \begin{bmatrix} \cos[k(z-z_0)] & \frac{nZ}{k}\sin[k(z-z_0)] \\ -\frac{k}{nZ}\sin[k(z-z_0)] & \cos[k(z-z_0)] \end{bmatrix}$$

and $\varphi(z_0)$ is defined as

$$\varphi(z_0) = \begin{bmatrix} E(z_0) \\ \frac{1}{nZ}\left(\frac{\partial E}{\partial z}\right)_{z=z_0} \end{bmatrix}.$$

For $z = (a_1 + a_2)/2$ and $z_0 = 0$, Eq. (5) can be derived as

$$\varphi\left(\frac{a_1+a_2}{2}\right) = TT\left(\frac{a_1}{2}, \frac{a_2}{2}\right)\varphi(0). \tag{6}$$

$TT(\frac{a_1}{2}, \frac{a_2}{2})$ satisfies the following:

$$TT\left(\frac{a_1}{2}, \frac{a_2}{2}\right) = TT_2\left(\frac{a_2}{2}\right)TT_1\left(\frac{a_1}{2}\right), \tag{7}$$

where $TT_2(a_2/2)$ and $TT_1(a_1/2)$ are written as

$$TT_2\left(\frac{a_2}{2}\right) = \begin{bmatrix} \cos\left(\frac{k_2a_2}{2}\right) & \frac{n_2Z_2}{k_2}\sin\left(\frac{a_2k_2}{2}\right) \\ -\frac{k_2}{n_2Z_2}\sin\left(\frac{a_2k_2}{2}\right) & \cos\left(\frac{a_2k_2}{2}\right) \end{bmatrix}, \tag{8}$$

$$TT_1\left(\frac{a_1}{2}\right) = \begin{bmatrix} \cos\left(\frac{k_1a_1}{2}\right) & \frac{Z_1n_1}{k_1}\sin\left(\frac{a_1k_1}{2}\right) \\ -\frac{k_1}{n_1Z_1}\sin\left(\frac{a_1k_1}{2}\right) & \cos\left(\frac{a_1k_1}{2}\right) \end{bmatrix}. \tag{9}$$

It is supposed that $TT\left(\frac{a_1}{2}, \frac{a_2}{2}\right) = \begin{bmatrix} TT1 & TT2 \\ TT3 & TT4 \end{bmatrix}$. Using Eq. (7), the elements of the matrix $TT(\frac{a_1}{2}, \frac{a_2}{2})$ can be derived as

$$TT1 = \cos\left(\frac{a_2k_2}{2}\right)\cos\left(\frac{a_1k_1}{2}\right) - \frac{Z_2n_2k_1}{Z_1n_1k_2}\sin\left(\frac{k_2a_2}{2}\right)\sin\left(\frac{k_1a_1}{2}\right), \tag{10}$$

$$TT2 = \frac{Z_1n_1}{k_1}\cos(\frac{a_2k_2}{2})\sin(\frac{a_1k_1}{2}) + \frac{Z_2n_2}{k_2}\sin\left(\frac{k_2a_2}{2}\right)\cos\left(\frac{k_1a_1}{2}\right), \tag{11}$$

$$TT3 = -\frac{k_2}{Z_2n_2}\sin(\frac{a_2k_2}{2})\cos(\frac{a_1k_1}{2}) - \frac{k_1}{Z_1n_1}\cos\left(\frac{k_2a_2}{2}\right)\sin\left(\frac{k_1a_1}{2}\right), \tag{12}$$

$$TT4 = \cos\left(\frac{a_2k_2}{2}\right)\cos\left(\frac{a_1k_1}{2}\right) - \frac{Z_1n_1k_2}{Z_2n_2k_1}\sin\left(\frac{k_2a_2}{2}\right)\sin\left(\frac{k_1a_1}{2}\right). \tag{13}$$

If the equations of

$$\varphi\left(-\frac{a_1+a_2}{2}\right) = TT\left(-\frac{a_1}{2}, -\frac{a_2}{2}\right)\varphi(0) \tag{14}$$

and

$$TT\left(-\frac{a_1}{2}, -\frac{a_2}{2}\right) = TT_2\left(-\frac{a_2}{2}\right)TT_1\left(-\frac{a_1}{2}\right) \tag{15}$$

are considered, one may obtain

$$TT\left(-\frac{a_1}{2}, -\frac{a_2}{2}\right) = \begin{bmatrix} TT1 & -TT2 \\ -TT3 & TT4 \end{bmatrix}. \tag{16}$$

If the Bloch condition

$$\varphi(z+a) = e^{iqa}\varphi(z) \tag{17}$$

is considered, then it can be derived that

$$\varphi\left(\frac{a_1+a_2}{2}\right) = \varphi\left(a - \frac{a_1+a_2}{2}\right) = e^{iqa}\varphi\left(-\frac{a_1+a_2}{2}\right), \tag{18}$$

where q is located in the Brillouin zone of the photonic superlattice with respect to $-m\pi \le q(a_1+a_2) \le m\pi$ ($m = 1, 2, 3, 4, \ldots$).

Using Eqs. (6), (14) and (18), it becomes

$$\varphi\left(\frac{a_1+a_2}{2}\right) = \begin{bmatrix} TT1 & TT2 \\ TT3 & TT4 \end{bmatrix}\varphi(0) = e^{iqa}\begin{bmatrix} TT1 & -TT2 \\ -TT3 & TT4 \end{bmatrix}\varphi(0) = e^{iqa}\varphi\left(-\frac{a_1+a_2}{2}\right), \tag{19}$$

which can be further generated as

$$\begin{bmatrix} TT1(1-e^{iqa}) & TT2(1+e^{iqa}) \\ TT3(1+e^{iqa}) & TT4(1-e^{iqa}) \end{bmatrix}\varphi(0) = 0. \tag{20}$$

To solve this secular equation, it should be satisfied that

$$TT1\,TT4(1-e^{iqa})^2 = TT2\,TT3(1+e^{iqa})^2. \tag{21}$$

From Eqs. (10)–(13), it can be derived that

$$TT1\,TT4 - TT2\,TT3 = 1. \tag{22}$$

Substituting Eq. (22) into Eq. (21), the following equations can be obtained:

$$TT2\,TT3 = \frac{\cos(qa)-1}{2}, \tag{23}$$

$$TT1\,TT4 = \frac{\cos(qa)+1}{2}, \tag{24}$$

$$q = \frac{1}{a}\arccos(2\,TT1\,TT4 - 1). \tag{25}$$

Substituting Eqs. (10)–(13) into Eq. (25), we are able to generate that

$$q = \frac{1}{a}\arccos(u), \tag{26}$$

where u takes the form

$$u = 2\cos^2\left(\frac{a_2k_2}{2}\right)\cos^2\left(\frac{a_1k_1}{2}\right) - \frac{1}{2}\left(\frac{Z_1n_1k_2}{Z_2n_2k_1} - \frac{Z_2n_2k_1}{Z_1n_1k_2}\right)\sin(a_1k_1)\sin(a_2k_2) + 2\sin^2\left(\frac{a_2k_2}{2}\right)\sin^2\left(\frac{a_1k_1}{2}\right) - 1. \tag{27}$$

The q-space volume is considered to be occupied by each wave vector point $V/(2\pi)^3$. The number of modes N covering frequencies from f to df is given by

$$N = Dd\omega = \left[\frac{V}{(2\pi)^3}\right]\int \mathrm{d}h\mathrm{d}S, \tag{28}$$

where dh is the small thickness and dS is the small area.

Considering the block wave confined in 1D space with unit area leads to the equation:

$$N(f) = \frac{L}{2\pi}\int \mathrm{d}h \approx \frac{Lq}{2\pi}. \tag{29}$$

The density of the states can be derived as

$$D(f) = \frac{L}{4\pi^2}\frac{\partial q}{\partial f}. \tag{30}$$

B. Lithium-Niobate-Based 1D Superlattices

In this case, the material in one layer is supposed to be lithium niobate, whose refractive index n_2 can be defined by [33]

$$n_2 = \sqrt{4.913 + \frac{0.0165T^2 + 117300}{\lambda^2 - (212 + 2.7\times10^{-5}T^2)^2} - 2.78\times10^{-8}\lambda^2}, \tag{31}$$

where λ is wavelength.

It can be noted that $k_1 = 2\pi f n_1/c$ and $k_2 = 2\pi f n_2/c$. In order to calculate the density of states via Eq. (27), the forms of $\frac{\partial n_2}{\partial f}$, $\frac{\partial k_1}{\partial f}$, and $\frac{\partial k_2}{\partial f}$ have to be obtained.

Their derivation of the frequency can be obtained:

$$\frac{\partial n_2}{\partial f} = \frac{1}{2}\left[4.913 + \frac{0.0165T^2f^2 + 117300f^2}{c^2 - f^2(212 + 2.7\times10^{-5}T^2)^2} - 2.78 \times 10^{-8}\frac{c^2}{f^2}\right]^{-\frac{1}{2}}\left\{\frac{(-0.033T^2 - 234600)c^2 f}{[c^2 - (212 + 2.7\times10^{-5}T^2)^2 f^2]^2} + 5.56\times10^{-8}c^2 f^{-3}\right\}, \tag{32}$$

$$\frac{\partial k_1}{\partial f} = \frac{2\pi n_1}{c}, \tag{33}$$

$$\frac{\partial k_2}{\partial f} = \frac{2\pi n_2}{c} + \frac{2\pi f}{c}\frac{\partial n_2}{\partial f}. \tag{34}$$

Using Eq. (30), the density of states D can be found:

$$D = \frac{L}{4\pi^2 a[1 - (2TT1TT4 - 1)^2]^{1/2}}\frac{\partial u}{\partial f}. \tag{35}$$

$\frac{\partial u}{\partial f}$ can be obtained:

$$\frac{\partial u}{\partial f} = \frac{\partial u_1}{\partial f} - \frac{\sin(a_1k_1)\sin(a_2k_2)}{2}\frac{\partial u_2}{\partial f} - \frac{u_2}{2}\frac{\partial u_3}{\partial f} + \frac{\partial u_4}{\partial f}, \tag{36}$$

u_1, u_2, u_3, and u_4 are defined in the following forms:

$$u_1 = 2\cos^2\left(\frac{a_2k_2}{2}\right)\cos^2\left(\frac{a_1k_1}{2}\right), \tag{37}$$

$$u_2 = \frac{Z_1n_1k_2}{Z_2n_2k_1} - \frac{Z_2n_2k_1}{Z_1n_1k_2}, \tag{38}$$

$$u_3 = \sin(a_1k_1)\sin(a_2k_2), \tag{39}$$

$$u_4 = 2\sin^2\left(\frac{a_2k_2}{2}\right)\sin^2\left(\frac{a_1k_1}{2}\right). \tag{40}$$

Their derivation is given by

$$\frac{\partial u_1}{\partial f} = -a_2\sin(a_2k_2)\cos^2\left(\frac{a_1k_1}{2}\right)\frac{\partial k_2}{\partial f}\cos^2\left(\frac{a_1k_1}{2}\right) - a_1\frac{\partial k_1}{\partial f}\cos^2\left(\frac{a_2k_2}{2}\right)\sin(a_1k_1), \tag{41}$$

$$\frac{\partial u_2}{\partial f} = \frac{Z_1n_1}{Z_2n_2k_1}\frac{\partial k_2}{\partial f} - \frac{Z_1n_1k_2}{Z_2}(n_2k_1)^{-2}\left(k_1\frac{\partial n_2}{\partial f} + n_2\frac{\partial k_1}{\partial f}\right) - \frac{Z_2k_1}{Z_1n_1k_2}\frac{\partial n_2}{\partial f} - \frac{Z_2n_2}{Z_1n_1}\left[\frac{1}{k_2}\frac{\partial k_1}{\partial f} - k_1k_2^{-2}\frac{\partial k_2}{\partial f}\right], \tag{42}$$

$$\frac{\partial u_3}{\partial f} = a_1\frac{\partial k_1}{\partial f}\cos(a_1k_1)\sin(a_2k_2) + a_2\frac{\partial k_2}{\partial f}\sin(a_1k_1)\cos(a_2k_2), \tag{43}$$

$$\frac{\partial u_4}{\partial f} = 2a_2\cos\left(\frac{a_2k_2}{2}\right)\sin^2\left(\frac{a_1k_1}{2}\right) + 2a_1\frac{\partial k_1}{\partial f}\sin^2\left(\frac{a_2k_2}{2}\right)\cos\left(\frac{a_1k_1}{2}\right), \tag{44}$$

$$\frac{\partial u}{\partial f} = \frac{\partial u_1}{\partial f} - \frac{\sin(a_1k_1)\sin(a_2k_2)}{2}\frac{\partial u_2}{\partial f} - \frac{u_2}{2}\frac{\partial u_3}{\partial f} + \frac{\partial u_4}{\partial f}. \tag{45}$$

C. Liquid-Crystal-Based Superlattices

In this case, the material in one layer is supposed to be liquid crystal, whose refractive index n_3 can be defined by [34]

$$n_3 = A - TB. \tag{46}$$

T is the temperature. A and B are constants given by the following forms:

$$A = \frac{7}{2\sqrt{10}} + \frac{2\sqrt{10}}{5}\frac{N_A\pi\langle\alpha\rangle A'}{M}, \tag{47}$$

$$B = \frac{2\sqrt{10}}{5}\frac{N_A\pi\langle\alpha\rangle B'}{M}, \tag{48}$$

where $\langle\alpha\rangle$ is average polarizability, M is molecular weight, N_A is Avogadro's number, and A' and B' are the constants given by the liquid crystal. The calculation of density of states is similar to that in Eqs. (31)–(45).

D. Zero-⟨n⟩ Condition

In this section, it should be pointed out that the zero-$\langle n\rangle$ condition [26–30], which stresses the existence of a zero-average-refractive-index gap in a photonic system, may be conveniently extended in order to find out the critical temperature associated with this gap. In fact, one may derive that

$$\langle k\rangle = \frac{1}{a_1 + a_2}\int_0^l k(T)\mathrm{d}l = \frac{1}{a_1 + a_2}[a_1k_1(T) - a_2k_2(T)] = 0, \tag{49}$$

where k is the wave vector and T is the value of the temperature when the spatial average wave vector value is zero. This equation illustrates that the temperature at which the spatial average wave vector, taken over a period of the photonic structure, vanishes. At this critical temperature, the corresponding effect of zero-$\langle n\rangle$ appears.

For a photonic structure that contains lithium niobate, by combing Eqs. (31) and (49), the critical temperature point can be solved.

In order to calculate the critical temperature, one may suppose that

$$X_1 = \left(\frac{{a_1}^2{n_1}^2}{{a_2}^2} + 2.78 \times 10^{-8}\frac{c^2}{f^2} - 4.91\right), \tag{50}$$

$$T_2 = \sqrt{14.58 \times 10^{-10} X_1}, \tag{51}$$

$$T_3 = (0.01X_1 + 0.02)^2 - 29.16 \times 10^{-10}$$

$$X_1\left(\frac{X_1 c^2}{f^2} - X_1 44944 - 117300\right), \tag{52}$$

$$T_1 = \sqrt{-(0.01X_1 + 0.02) + \sqrt{T_3}}. \tag{53}$$

The corresponding temperature T_{c1} can be expressed as

$$T_{c1} = T_1/T_2. \tag{54}$$

For a photonic structure that contains liquid crystals, the temperature can be derived through Eqs. (46) and (49) as

$$T_{c2} = \frac{(A - a_1 n_1/a_2)}{B}. \tag{55}$$

As can be seen from Eqs. (50)–(55), the refractive index (n_1) and layer width ratio (a_1/a_2) can be used to calculate the value of the temperature such that $\langle n\rangle$ vanishes.

E. Null-Gap Condition

From Eqs. (23), (24), it can be noted that the extrema of the photonic band can be generated from the choice that $\cos(qa) = 1$ or $\cos(qa) = -1$. When the condition of $\cos(qa) = 1$ is satisfied, it can be derived that $TT2 = 0$ or $TT3 = 0$. When the choice of $\cos(qa) = -1$ is made, it can be generated that $TT1 = 0$ or $TT4 = 0$. At those values of the temperature, the bands vanish. If one considers that $TT2 = TT3 = 0$ or $TT1 = TT4 = 0$, it implies the touching of the bands.

We select the condition $TT2 = TT3 = 0$ for calculation of the values of the temperature corresponding to the null gap.

From the equation $TT2 = TT3 = 0$, we are able to derive the following: $\sin(a_2k_2/2) = 0$ and $\sin(a_1k_1/2) = 0$. Therefore, $a_2k_2/2 = N_2\pi$, $a_1k_1/2 = N_1\pi$. Here N_1 and N_2 satisfy $N_1 = \ldots, -3\pi, -2\pi, -\pi, \pi, 2\pi, 3\pi, \ldots$ and $N_2 = \ldots, -3\pi, -2\pi, -\pi, \pi, 2\pi, 3\pi, \ldots$. Zero values of N_1 and N_2 are ignored for simple calculation. It can be noted that $k_1 = \omega n_1/c, k_2 = \omega n_2/c$.

For the superlattices based on lithium niobate or liquid crystal, it can be obtained that

$$n_2 = a_1 n_1 N_2/a_2/N_1, \tag{56}$$

$$n_3 = a_1 n_1 N_3/a_2/N_1, \tag{57}$$

where $N_3 = \ldots, -3\pi, -2\pi, -\pi, \pi, 2\pi, 3\pi, \ldots$.

Based on Eqs. (56), (57), (31), and (46), the values of the temperature corresponding to the null gap of the superlattices can be written as

$$T_{ng1} = \sqrt{\frac{(t_2 \pm \sqrt{{t_2}^2 - 29.16 \times 10^{-10} t_1 t_3})}{14.58 \times 10^{-10} t_1}}, \tag{58}$$

$$T_{ng2} = \frac{A}{B} - \frac{a_1 n_1 N_3}{a_2 N_1 B}, \tag{59}$$

where T_{ng1} is the temperature associated with the null gap for the lithium-niobate-based superlattices and T_{ng2} is for the liquid-crystal-based superlattices; t_1, t_2, and t_3 respectively take the forms

$$t_1 = \frac{{a_1}^2{n_1}^2{N_2}^2}{{a_2}^2{N_1}^2} - 4.91 + 2.78 \times 10^{-8}\lambda^2, \tag{60}$$

$$t_2 = 0.12 + 1144.8t_1 \times 10^{-5}, \tag{61}$$

$$t_3 = t_1\lambda^2 - 44944t_1 - 117300. \tag{62}$$

A moment's thought about Eqs. (58)–(62) implies that the values of the temperature corresponding to the null gap (T_{ng1} and T_{ng2}) can be determined by the refractive index (n_1) and the ratio of the layer width (a_1/a_2).

F. Concurrence of Zero-$\langle n\rangle$ and Null Gap

From Eq. (49), it can be derived that the occurrence of the zero-$\langle n\rangle$ for the lithium-niobate-based superlattices is associated with the condition of $a_1n_1 = a_2n_2$.

From Section 2.D, it can be obtained that the null gap happens when $a_1n_1N_2 = a_2n_2N_1$ is satisfied.

Therefore, the concurrence of zero-$\langle n\rangle$ and null gap for the lithium-niobate-based superlattices implies that $a_1n_1 = a_2n_2$ and $N_2 = N_1$. For the liquid-crystal-based superlattices, this indicates that $a_1n_1 = a_2n_3$ and $N_3 = N_1$.

We are interested in the study of optical waves or electromagnetic waves with high frequency, at which the zero-$\langle n\rangle$ and null gap can happen simultaneously. With this consideration, Eq. (31) can be simplified as

$$n_2 = \sqrt{4.913 - \frac{0.0165T^2 + 117300}{(212 + 2.7 \times 10^{-5}T^2)^2}}. \tag{63}$$

Using the equations of $k_2 = \omega n_2/c$, $a_2k_2/2 = N_2\pi$, it can be derived that the propagation wavelength with respect to the concurrence of zero-$\langle n\rangle$ and null gap in the lithium-niobate-based superlattices satisfies

$$\lambda_2 = a_2n_2/N_2. \tag{64}$$

Substituting Eq. (63) into Eq. (64), it can be written that

$$\lambda_2 = \frac{a_2}{N_2}\sqrt{4.913 - \frac{0.0165T^2 + 117300}{(212 + 2.7 \times 10^{-5}T^2)^2}}. \tag{65}$$

Similarly, the propagation wavelength with respect to the concurrence of zero-$\langle n\rangle$ and null gap in the liquid-crystal-based superlattices can be obtained as

$$\lambda_3 = \frac{a_2}{N_3}(A - TB). \tag{66}$$

Equations (65) and (66) give the explicit expressions of λ_2 and λ_3 in terms of temperature. Again, this indicates that the temperature can impact the concurrence of zero-$\langle n \rangle$ and null gap.

3. RESULTS AND DISCUSSION

Our numerical calculations are focused on two types of 1D photonic superlattices. The first one is based on a medium A with the refractive index n_1 and a medium B made from lithium niobate (ABABABAB... stack). The second one is based on medium A and a medium C made fromliquid crystal (ACACACAC... stack). In this section, explicit discussions on band structure, density of states, and concurrence of zero-$\langle n \rangle$ and null gap for them in terms of temperature are presented.

A. Band Structures and Density of States of Lithium-Niobate-Based Superlattices

The photonic band structures of a 1D superlattice based on lithium niobate of period a are displayed in Fig. 1 for various refractive indices of the layer, illustrating the presence of gaps in the band structures. In the temperature range around 0–250 K, the dispersion curves are close for $n_1 = 0.5$. When $n_1 = 1.5$, the dispersion curves start to open. They suggest that the dispersion curves are open with higher refractive index. Figure 2 depicts the results of the corresponding photon density of states (DOS). For $n_1 = 0.5$, the values of DOS are around 0–3; for $n_1 = 1.5$, the values of DOS are around 0–4; for $n_1 = 3.5$, the values of DOS are around 0–10. These results illustrate that, for greater refractive index, the corresponding dispersion curves become more scattered and the photon density of states is greater.

It can be noted that for $n_1 = 0.5$, qa shows the zeroth values attemperatures around 33 K, 276 K, 287 K, 397 K, 408 K, 498 K, and 578 K [Fig. 1(a)]. The curves of the DOS show sharp peaks at temperatures around 30 K, 184 K, 205 K, 273 K, 288 K, 342 K, 352 K, 398 K, 409 K, 448 K, 456 K, 491 K, 501 K, 533 K, 543 K, 575 K, and 580 K [Fig. 2(a)]. For $n_1 = 1.5$, qa becomes zero at temperatures around 247 K, 281 K, 380 K, 402 K, 477 K, 496 K, 560 K, and 577 K [Fig. 1(b)]. The peak values of DOS are presented at several temperature points of 144 K, 192 K, 247 K, 279 K, 320 K, 345 K, 378 K, 402 K, 431 K, 450 K, 478 K, 494 K, 520 K, 537 K, 561 K, 576 K, and 597 K [Fig. 2(b)]. For $n_1 = 3.5$, qa becomes zero at temperatures around 219 K, 248 K, 360 K, 379 K, 463 K, 478 K, 547 K, and 562 K [Fig. 1(c)]. The DOS has maxima values at 86 K, 144 K, 219 K, 247 K, 298 K, 320 K, 358 K, 381 K, 413 K, 431 K, 462 K, 478 K, 508 K, 521 K, 547 K, 561 K, 584 K, and 600 K [Fig. 2(c)].

The modifications introduced in the photonic band structures and photon density of states, when different layer widths are used, are illustrated in Figs. 3 and 4.

Figure 3(a) reveals that the values of qa become zero at the temperature of 592 K with $a_2 = 2.185$ μm. Figure 3(b) illustrates a few sets of dispersion curves. Moreover, the values of qa become null at the temperatures of 153 K, 380 K, and 518 K. Figure 3(c) shows very dense sets of data curves with $a_2 = 50$ μm. It can be seen that qa shows zeroth values at temperatures of 153 K, 218 K, 267 K, 308 K, 345 K, 378 K, 409 K, 437 K, 465 K, 491 K, 516 K, 538 K, 562 K, and 584 K.

In Fig. 4(a), the DOS curves show one distinct peak around 257 K. In Fig. 4(b), the DOS curves illustrate three distinct

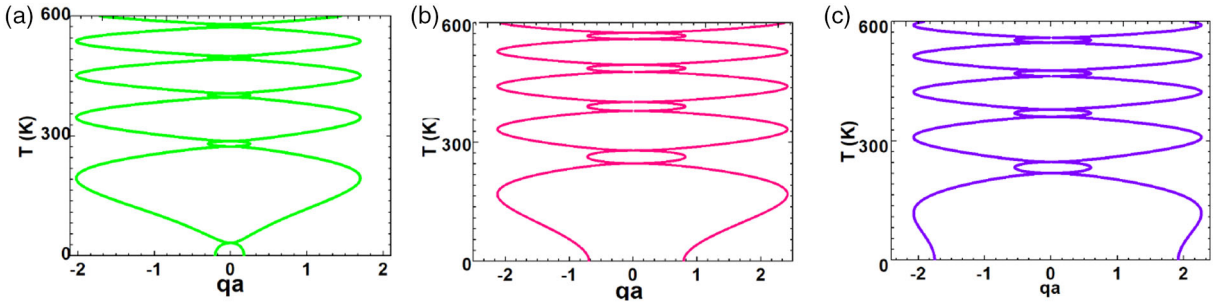

Fig. 1. Temperature-adjustable band structure of lithium-niobate-based superlattices with different layer refractive indices: (a) $n_1 = 0.5$, (b) $n_1 = 1.5$, (c) $n_1 = 3.5$.

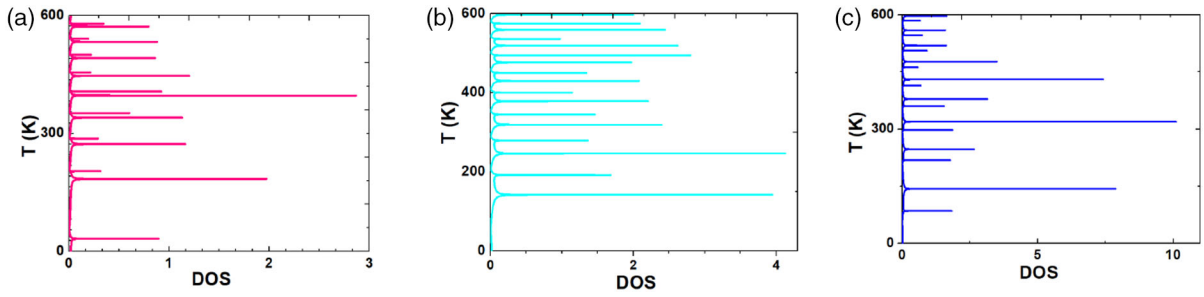

Fig. 2. Temperature-adjustable density of states of lithium-niobate-based superlattices with different layer refractive indices: (a) $n_1 = 0.5$, (b) $n_1 = 1.5$, (c) $n_1 = 3.5$.

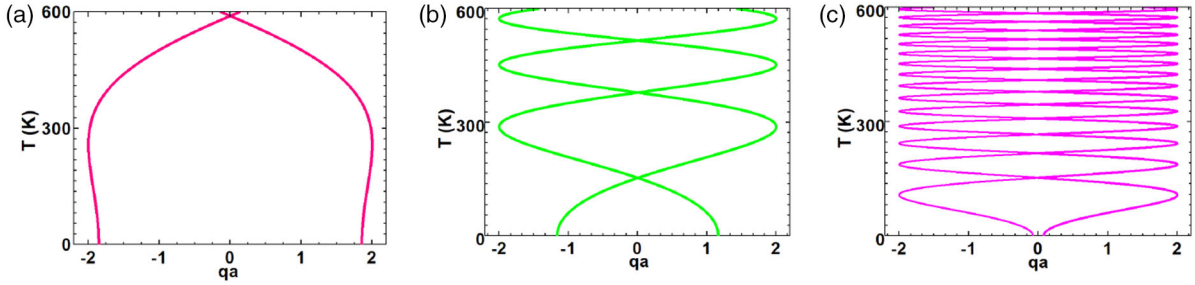

Fig. 3. Temperature-adjustable band structure of lithium-niobate-based superlattices with different layer thicknesses: (a) $a_2 = 2.185$ μm, (b) $a_2 = 10$ μm, (c) $a_2 = 50$ μm.

peaks at 285 K, 451 K, and 574 K. In Fig. 4(c), the DOS curves reveal several peaks around 105 K, 187 K, 243 K, 287 K, 327 K, 360 K, 393 K, 424 K, 452 K, 478 K, 505 K, 527 K, 551 K, 574 K, and 595 K.

One clearly sees that, for narrower layers, the corresponding dispersion curves and photonic density of states become fewer and more scattered.

It is interesting to find out the impact of propagation wavelength on the photonic band structures and photon density of states in Figs. 5 and 6.

When the propagation wavelength λ is equal to 350 nm, the zeroth values of qa appear at temperatures around 155 K, 252 K, 320 K, 379 K, 431 K, 476 K, 516 K, 556 K, and 594 K [Fig. 5(a)]. The peak values of DOS are shown at temperatures around 61 K, 207 K, 287 K, 352 K, 404 K, 452 K, 495 K, 537 K, and 575 K [Fig. 6(a)].

For λ = 532 nm, the zeroth values of qa are presented at temperatures around 36 K, 215 K, 250 K, 328 K, 350 K, 413 K, 430 K, 483 K, 498 K, 546 K, 558 K, and 596 K [Fig. 5(b)]. The peak values of DOS are shown at temperatures around 35 K, 134 K, 177 K, 219 K, 248 K, 281 K, 304 K, 329 K, 350 K, 373 K, 392 K, 412 K, 431 K, 448 K, 467 K, 483 K, 496 K, 514 K, 529 K, 544 K, 556 K, 573 K, and 587 K [Fig. 6(b)].

For λ = 1064 nm, the zeroth values of qa are revealed at temperatures around 43 K, 322 K, 352 K, 477 K, 498 K, and 594 K [Fig. 5(c)]. The peak values of DOS are presented at temperatures around 43 K, 207 K, 250 K, 322 K, 350 K, 406 K, 429 K, 476 K, 498 K, 538 K, 557 K, and 595 K [Fig. 6(c)]. Comparison of Figs. 5(a)–5(c) clearly shows that the dispersion curves become sparser for the longer propagation wavelength.

B. Band Structure and Density of States of Liquid-Crystal-Based Superlattices

The variation of refractive index, layer width, and propagation wavelength can have impact on the photonic band for liquid-crystal-based superlattices.

Figure 7 depicts the band structures in accordance with different refractive indices. For $n_1 = 0.5$, qa is approaching zero when T is around 102 K, 281 K, and 461 K [Fig. 7(a)]. For

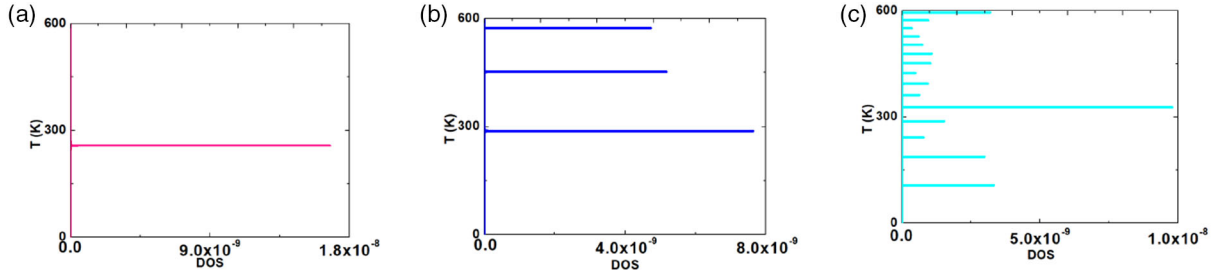

Fig. 4. Temperature-adjustable density of states of lithium-niobate-based superlattices with different layer thicknesses: (a) $a_2 = 2.185$ μm, (b) $a_2 = 10$ μm, (c) $a_2 = 50$ μm.

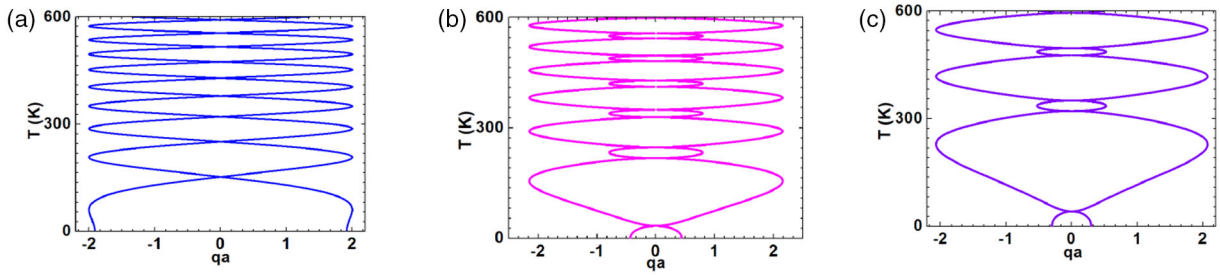

Fig. 5. Temperature-adjustable band structure of lithium-niobate-based superlattices with various values of propagation wavelength: (a) λ = 350 nm, (b) λ = 532 nm, (c) λ = 1064 nm.

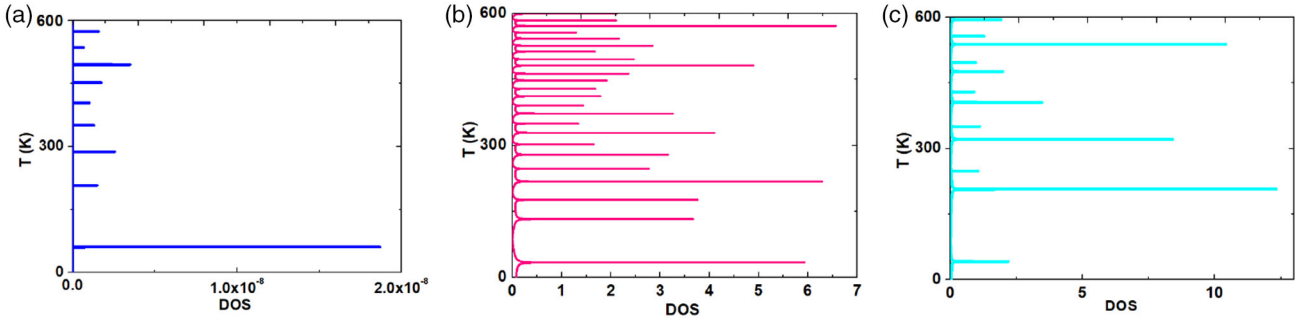

Fig. 6. Temperature-adjustable density of states of lithium-niobate-based supperlattices with various values of propagation wavelength: (a) $\lambda = 350$ nm, (b) $\lambda = 532$ nm, (b) $\lambda = 1064$ nm.

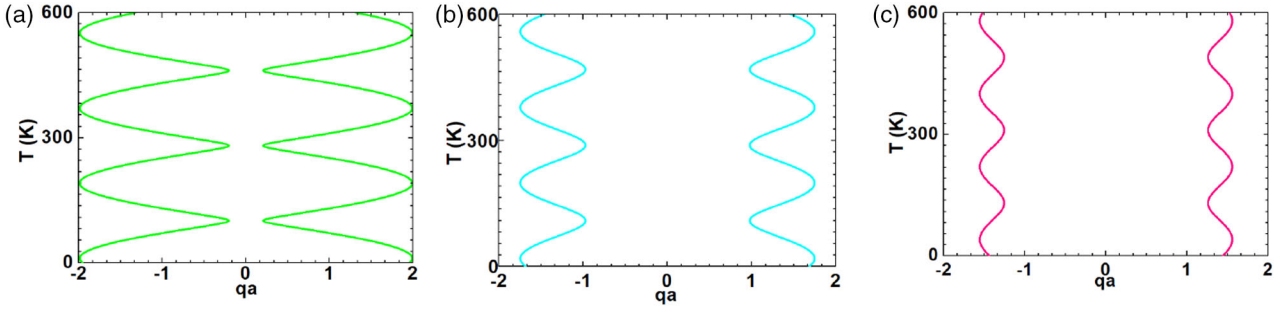

Fig. 7. Temperature-adjustable band structure of liquid-crystal-based superlattices with respect to a varied layer refractive index: (a) $n_1 = 0.5$, (b) $n_1 = 2.5$, (c) $n_1 = 3.5$.

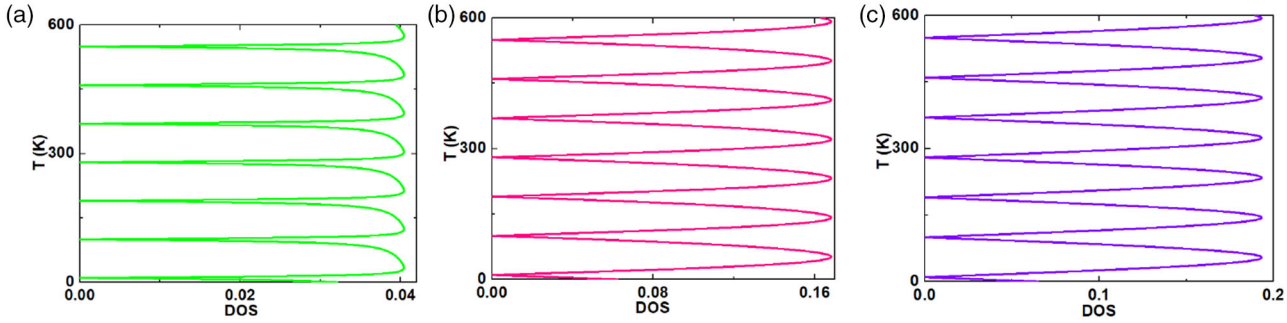

Fig. 8. Temperature-adjustable density of states of liquid-crystal-based superlattices with respect to different layer refractive indices: (a) $n_1 = 0.5$, (b) $n_1 = 2.5$, (c) $n_1 = 3.5$.

$n_1 = 2.5$ or $n_1 = 3.5$, the left and right sets of the dispersion curves are separated far from each other [Figs. 7(b) and 7(c)].

Figure 8(a) reveals the values of the DOS are around 0–0.04 for $n_1 = 0.5$. The maximum value of the DOS is 0.04, which appears at several temperature points of 34 K, 126 K, 214 K, 303 K, 395 K, 485 K, and 577 K [Fig. 8(a)]. Figure 8(b) shows that the values of the DOS are around 0–0.18 for $n_1 = 2.5$. The peak value of the DOS is 0.18, which shows at the temperature points of 54 K, 145 K, 233 K, 324 K, 413 K, 504 K, and 593 K [Fig. 8(b)]. For $n_1 = 3.5$, the values of the DOS are around 0–0.19 [Fig. 8(c)]. The maximum value of the DOS is 0.19, which presents at $T = 56$ K, 147 K, 237 K, 326 K, 416 K, 505 K, and 595 K [Fig. 8(c)].

These results imply that the higher photonic DOS is associated with higher refractive index for the liquid-crystal-based superlattices.

The changes introduced in the photonic band structure and photon DOS, when different layer widths are used, are illustrated in Figs. 9 and 10. Figure 9(a) illustrates that for $a_2 = 10$ nm, the values of qa become zero when T is 551 K. Also, the values of the DOS present distinct peaks when T is 100 K and 551 K [Fig. 10(a)]. Figure 9(b) reveals that for $a_2 = 30$ nm, the values of qa take zero when T is 253 K and 553 K. Moreover, the values of DOS show four peaks at $T = 99$ K, 250 K, 399 K, and 550 K [Fig. 10(b)]. It can be seen from Fig. 9(c) that for $a_2 = 50$ nm, the zeroth values of qa appear when T is 10 K, 192 K, 371 K, and 550 K. Correspondingly, the peak values of DOS are presented at $T = 11$ K, 101 K, 190 K, 280 K, 370 K, 459 K, and 550 K.

One clearly sees that, for narrower layers, the corresponding dispersion curves become fewer and the photonic DOSs become sparser.

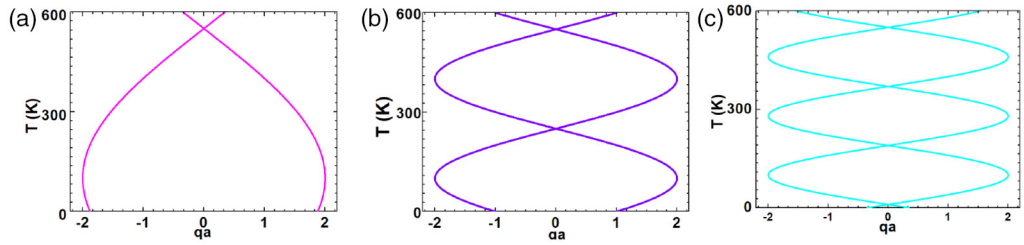

Fig. 9. Temperature-adjustable band structure of liquid-crystal-based supperlattices with respect to different layer thicknesses: (a) $a_2 = 10$ nm, (b) $a_2 = 30$ nm, (b) $a_2 = 50$ nm.

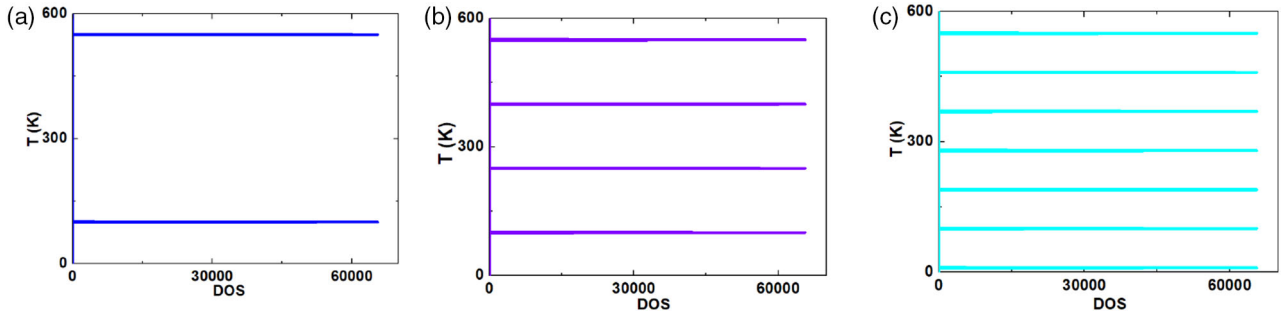

Fig. 10. Temperature-adjustable density of states of liquid-crystal-based supperlattices with respect to different layer thicknesses: (a) $a_2 = 10$ nm, (b) $a_2 = 30$ nm, (c) $a_2 = 50$ nm.

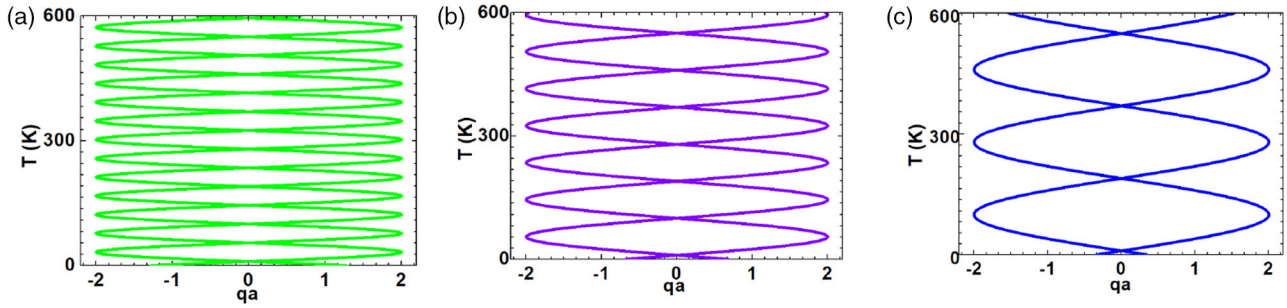

Fig. 11. Temperature-adjustable band structure of liquid-crystal-based superlattices corresponding to different propagation wavelengths: (a) $\lambda = 225$ nm, (b) $\lambda = 450$ nm, (c) $\lambda = 900$ nm.

The impact introduced in the photonic band structure and photon DOS, when different propagation wavelengths are used, is illustrated in Figs. 11 and 12.

It can be found in Fig. 11(a) that when λ is 225 nm, the zeroth values of qa are presented at the temperature points of 10 K, 56 K, 101 K, 146 K, 192 K, 238 K, 281 K, 326 K, 371 K, 416 K, 462 K, 507 K, 551 K, and 595 K. Moreover, the values of the DOS reveal peaks at 11 K, 55 K, 100 K,146 K, 190 K, 234 K, 280 K, 324 K, 371 K, 415 K, 459 K, 505 K, 549 K, and 595 K [Fig. 12(a)].

Figure 11(b) reveals that when λ is 450 nm, the zeroth values of qa appear when T is 10 K, 101 K, 191 K, 281 K, 370 K, 462 K, and 551 K. The values of the DOS show distinct peaks at 11 K, 54 K, 99 K, 144 K, 190 K, 234 K, 281 K, 325 K, 370 K, 415 K, 459 K, 504 K, 550 K, and 596 K.

Figure 11(c) illustrates that when λ is 900 nm, the zeroth values of qa appear when T is 11 K, 189 K, 371 K, and 551 K. Accordingly, the peak values of the DOS appear at 11 K, 102 K, 190 K, 279 K, 369 K, 459 K, and 549 K [Fig. 12(c)]. It can be noted that, for smaller wavelength, the corresponding dispersion curves become more intensive and the photonic DOSs become sparser.

C. Temperature Values Corresponding to the Zero-⟨n⟩ and Null Gap

The relationship between T_{c1} and T_{c2} and the refractive index (n_1) as well as the ratio of the layer width (a_1/a_2) is investigated.

Figure 13(a) illustrates the impact of a_1/a_2 on T_{c1} with various values of n_1. When n_1 is 1, T_{c1} shows the trend of first increasing and then decreasing with a_1/a_2 increasing, which presents a transition at $a_1/a_2 = 2.1$. When n_1 is 1.5, T_{c1} first increases and then decreases, which reveals the transition at $a_1/a_2 = 1.4$. When n_1 is 2 or 3.5, T_{c1} is suppressed when a_1/a_2 increases.

Figure 13(b) shows the trend of n_1 versus T_{c1} with different values of a_1/a_2. When a_1/a_2 is 0.5, T_{c1} shows the trend of first increasing and then decreasing with n_1 increasing, which shows

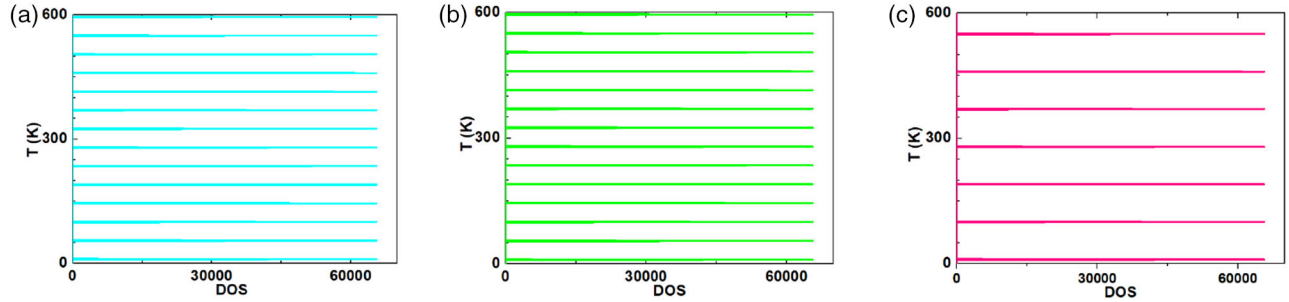

Fig. 12. Density of states of liquid-crystal-based superlattices with respect to different wavelengths: (a) $\lambda = 225$ nm, (b) $\lambda = 450$ nm, (c) $\lambda = 900$ nm.

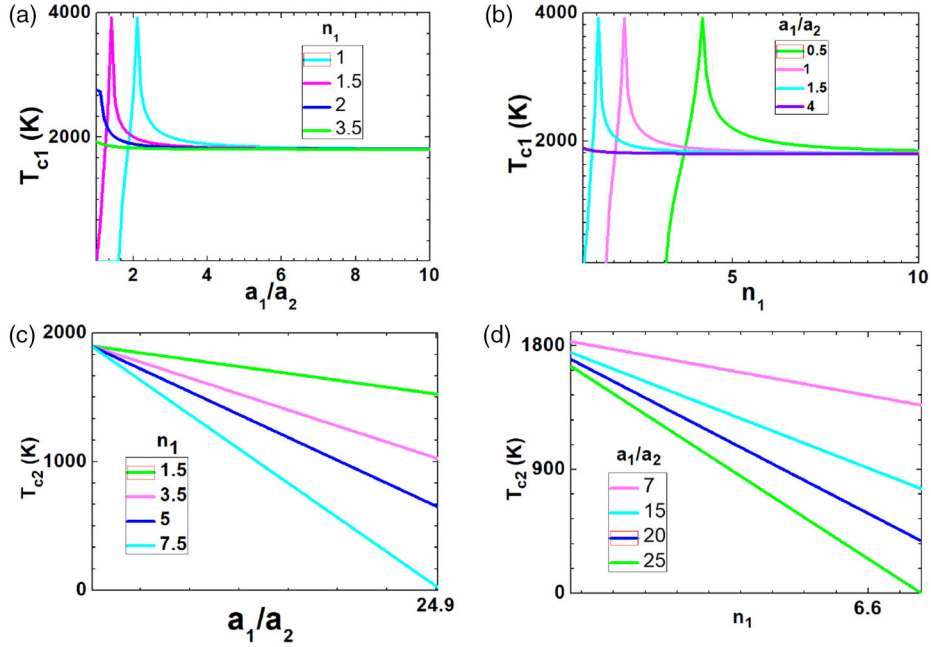

Fig. 13. Critical temperature point (T_{c1} and T_{c2}) dependence on the layer width ratio, refractive index, and frequency. (a) T_{c1} versus a_1/a_2 with various values of n_1. (b) T_{c1} versus n_1 with various values of a_1/a_2. (c) T_{c2} versus a_1/a_2 with various values of n_1. (d) T_{c2} versus n_1 with various a_1/a_2.

a transition at $n_1 = 4.2$. When a_1/a_2 is 1, T_{c1} first increases and then decreases, which reveals the transition at $n_1 = 2.1$. When a_1/a_2 is 1.5, T_{c1} first increases and then decreases, which transitions at $n_1 = 1.4$. When a_1/a_2 is 4, T_{c1} is suppressed when a_1/a_2 is increasing.

Figures 13(c) and 13(d) reveal that T_{c1} drops with either a_1/a_2 or n_1 increasing. The dropping rate is dependent on n_1 or a_1/a_2.

Figures 14(a)–14(d) indicate that T_{ng1} and T_{ng2} are suppressed when n_1 or a_1/a_2 is enhanced. These indicate that the temperature at which the zero-$\langle n \rangle$ or null gap appears can be related to the refractive index and the ratio of the layer width. These parameters decide how high the temperature should be operated in order to reach zero-$\langle n \rangle$ or null gap. In practical applications, an operational temperature lower than 600 K can be easy to achieve through some commercial hot plates. Temperatures higher than 600 K can be reached by using some furnaces. Nevertheless, zero-$\langle n \rangle$ or null gap can appear in the lithium-niobate-based or liquid-crystal-based superlattices via the modulation of the temperature.

Also, it should be noted that the concurrence of null gap and zero-$\langle n \rangle$ can be achieved at certain wavelength points, which can be modulated by the temperature. As shown in Fig. 15(a), the concurrence of null gap and zero-$\langle n \rangle$ in the lithium-niobate-based superlattices can be achieved at the wavelength points of 450–664 nm when T is increasing from 68 K to 29,893 K, which falls in the range of visible light. For the liquid-crystal-based superlattices, the wavelength corresponding to the concurrence of the null gap and zero-$\langle n \rangle$ decreases from 2278 nm to 361 nm when T increases from 1 K to 1600 K [see Fig. 15(b)].

They show the potential of using the temperature treatment to accomplish the concurrence of zero-$\langle n \rangle$ and null gap in superlattices in the visible optical range. For the lithium-niobate-based superlattices, the concurrence of zero-$\langle n \rangle$ and null gap in the blue light range requires control of the temperature around 376–1341 K [Fig. 15(a)]. For the liquid-crystal-based superlattices, the concurrence of zero-$\langle n \rangle$ and null gap in the blue/green/red light range requires the control of the temperature around 1340–1600 K [Fig. 15(b)].

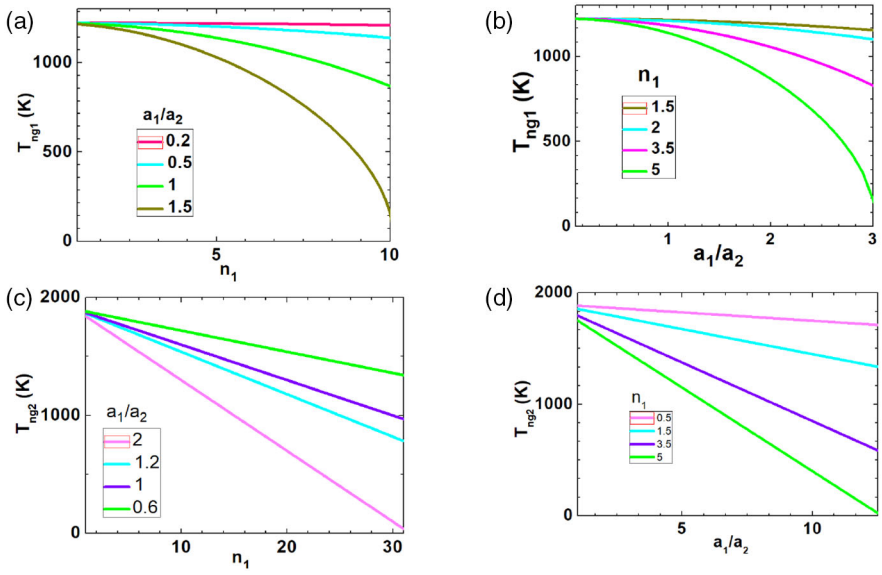

Fig. 14. Values of temperature corresponding to null gap (T_{ng1} and T_{ng2}) dependence on the layer width ratio and refractive index. (a) T_{ng1} versus n_1 with various a_1/a_2. (b) T_{ng1} versus a_1/a_2 with various n_1. (c) T_{ng2} versus n_1 with various a_1/a_2. (d) T_{ng2} versus a_1/a_2 with various n_1.

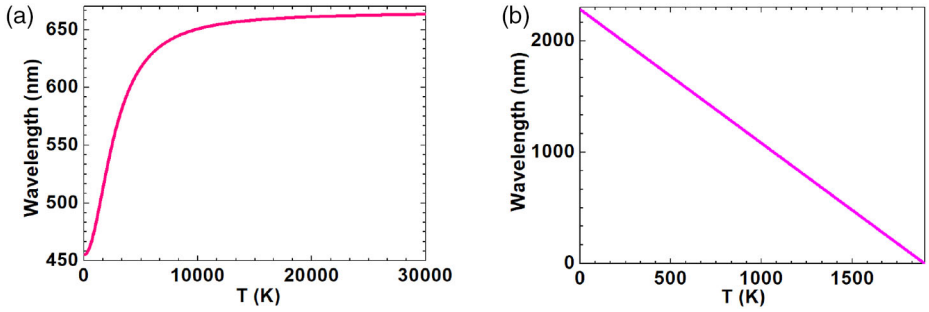

Fig. 15. Concurrence of null gap and zero-$\langle n\rangle$ in the superlattices can be achieved at certain wavelength points, which can be modulated by the temperature: (a) wavelength versus temperature for lithium-niobate-based superlattices; (b) wavelength versus temperature for liquid-crystal-based superlattices.

A moment's review of Eqs. (26), (30), (49), (58), (59), (65), and (66) shows that the photonic band, DOS, null gap, zero-$\langle n\rangle$, and concurrence of the null gap and zero-$\langle n\rangle$ are all associated with the temperature. For instance, the tuning of the band structure and DOS is done in the temperature range of 0–600 K. Also, it is able to achieve the null photonic gap at certain temperature points, which are decided by the ratio of layer width and the refractive index. Furthermore, it is illustrated that the spatial average of the wave vector $\langle k\rangle$ becomes null at a specific temperature, depending on the layer thickness and refractive index. The values of the temperature corresponding to zero-$\langle n\rangle$ are exhibited to be suppressed when the refractive index or the ratio of the layer width is increased. It especially is incredible to see how the null gap runs in parallel with zero-$\langle n\rangle$ at specific optical wavelengths, which are temperature dependent. It means that the physics of dispersion and the concept of the effective refractive index are intimately related.

Since these optical properties are found to be partially impacted by the thickness and refractive index of the materials, it will suffice to consider the effective handling of these optical properties with the design of device dimensions and the choice of layer refractive index.

Since the beginning of metamaterial study, the physics of zero-$\langle n\rangle$ have attracted the attention of the scientific community, including wavelength expansion, the geometry-invariant wave phenomena, and wave tunneling through deformed waveguides [26–32,35]. Traditional technologies for introducing zero-$\langle n\rangle$ are built upon the collection of dispersive permittivity of different materials, which can cross zero at a specific wavelength. Our study brings new knowledge to this field. In our findings, zero-$\langle n\rangle$ is associated with the temperature in 1D superlattices made from lithium niobate or liquid crystal. Furthermore, Eqs. (50)–(55) and the results presented in Fig. 14 clearly indicate that the temperature corresponding to the existance of zero-$\langle n\rangle$ is in close relation with the values of n_1 and a_1/a_2. These two parameters place some limitations on the design of lithium niobate or liquid crystal based 1D superlattices for introducing zero-$\langle n\rangle$ through the tuning of the temperature. Nevertheless, new devices may be fabricated to show a near-zero effective refractive index with our methods. A number of examples of near-zero-$\langle n\rangle$ technologies can be expected to be realized

by exploiting the properties of these 1D supperlattices. One example would be reconfigurable and smart surfaces, whose near-zero-$\langle n \rangle$ can be switched on or off by the rising or falling of the temperature.

It is worth mentioning that Eq. (2), the Maxwell's equation derivative, has related the refractive index with the electrical field or the layer thickness or the propagation wavelength. Given that the refractive index is dependent on the temperature in these two material systems we have proposed, there may be values of the temperature that can make the corresponding band structure and density of states resonant. At those values of the layer thickness or the propagation wavelength or the refractive index associated with the temperature, the coupling between the optical field and band structure may be strong enough, and the wave inside the waveguide could correspond to the coupled modes occurring throughout the whole material systems. Such a coupling may lead to the specific propagation of the optical field in a fierce way. This gives rise to those effects as illustrated, where the band structures and the density of states are shown to be adjustable by the temperature along with various values of the propagation wavelength, the refractive index, and the layer width.

The modification of the band structure is an important subject in this work, which proposes a temperature-adjusting approach. It should be noted that other approaches turned out to be beneficial, including the configuration of the defects [15], the changing of the pattern of veins or the type of rods in the photonic structure [18].

In many practical situations, the controlling of the optical band, DOS, null gap, and zero-$\langle n \rangle$ come together in a way that can be accomplished through the engineering of the metamaterials [26–32]. When it comes to the scope of the visible light, this is generally not easy to achieve experimentally, which may require the use of advanced optical lithography. It is useful therefore to seek an alternative solution that is facile and cheap to operate.

The understanding of these optical properties needs development. Our method of using temperature-controllable-refractive-index materials provides deep understanding of these optical properties in terms of the temperature. Furthermore, since the temperature is easy to manipulate in any modern lab, our investigation gives a solution of controlling these optical properties. Future developments may use the technique of laser-micromachining to inscribe micro-channels in certain substrates for filling the lithium niobate powders or liquid crystal molecules to implement such 1D superlattices.

4. CONCLUSIONS

We have analytically studied the temperature-variable photonic band structures and the DOSs of the superlattices consisting of layers made from lithium niobate or liquid crystal, whose refractive index is temperature sensitive. The band structures and the DOSs are found to be controllable by the temperature with various values of the propagation wavelength, the refractive index, and the layer width. The values of the temperature where zero-$\langle n \rangle$ is presented are found to be associated with the propagation wavelength, refractive index, and layer width. It is shown that a null photonic gap appears at certain temperature points, which are decided by the ratio of the layer width and the refractive index. The spatial average of the refractive index $\langle n \rangle$ vanishes at specific values of the temperature as functions of the refractive index and the ratio of the layer width. The null photonic gap and zero-$\langle n \rangle$ can show up simultaneously at certain wavelengths in the visible optical range. These values of the wavelength are dependent on the temperature. This study indicates that the introduction of lithium niobate or liquid crystal in the design of 1D superlattices is meaningful. It provides the flexible construction of optical material systems whose optical bands, null gap, and zero-$\langle n \rangle$ can be adjustable via the temperature.

Funding. National Key R&D Program of China (2017YFB 1103202); Jiangsu State R&D Program (BE2018010); Chongqing Research Program of Basic Research and Frontier Technology (cstc2017jcyjAX0469).

Acknowledgment. Special thanks to Ms. Jiangqi Luo and Dr. Hao Fu for offering help and valuable discussions.

Disclosures. The authors declare no conflicts of interest.

REFERENCES

1. H. Ren, S. Xu, and S.-T. Wu, "Gradient polymer network liquid crystal with a large refractive index change," Opt. Express **20**, 26464–26472 (2012).
2. G. Pawlik, W. Walasik, M. Jarema, A. C. Mitus, and I. Choon Khoo, "Temperature dependence of refractive index gradient in nanosphere dispersed liquid crystal (NDLC) metamaterial at infrared frequencies: Monte Carlo study," Opt. Mater. **34**, 1656–1659 (2012).
3. N. A. Elmahdy, M. S. Esmail, and M. M. El-Okr, "Characterization of a thermal sensor based on one-dimensional photonic crystal with central liquid crystal defect," Optik **170**, 444–451 (2018).
4. N. Xie, H. Zhang, B. Liu, B. Song, and J. Wu, " Characterization of temperature-dependent refractive indices for nematic liquid crystal employing a microfiber-assisted Mach-Zehnder interferometer," J. Lightwave Technol. **35**, 2966–2972 (2017).
5. C.-W. Chen, H.-C. Jau, C.-H. Lee, C.-C. Li, C.-T. Hou, C.-W. Wu, T.-H. Lin, and I. C. Khoo, "Temperature dependence of refractive index blue phase liquid crystals," Opt. Mater. Express **3**, 527–532 (2013).
6. V. V. Filippov, I. T. Bondar, N. V. Kuleshov, N. I. Leonyuk, V. V. Mal'tsev, and O. V. Pilipenko, "Dispersion and temperature dependence of the refractive indices of pure and Yb^{3+}-doped crystals of $YAl_3(BO_3)_4$," J. Opt. Technol. **74**, 717–719 (2007).
7. H. C. Liang, K. Y. Lin, Y. C. Lee, and Y. F. Chen, "Precise measurement of group refractive indices and temperature dependence of refractive index for Nd-doped yttrium orthovanadate by intracavity spontaneous mode locking," Opt. Lett. **36**, 3741–3743 (2011).
8. I. T. Bondar, V. M. Trukhan, and A. U. Sheleg, "Anisotropy of the temperature dependence of the refractive indices of a cadmium diphosphide crystal," J. Opt. Technol. **73**, 525–527 (2006).
9. R. Radhakrishnan, L. Gallais, and S. Monneret, "Wavefront sensing applied to determine the temperature dependence of the refractive index of liquids," Appl. Opt. **58**, 3646–3651 (2019).
10. L. M. Averina and Yu. S. Milyavskii, "Temperature dependence of the refractive index of acrylate elastomers," J. Opt. Technol. **71**, 249–250 (2004).
11. I. T. Bodnar and A. U. Sheleg, "Refractive indices of potassium titanyl phosphate: dispersion and temperature dependence," J. Opt. Technol. **70**, 673–675 (2003).
12. J. Li, S. Gauzia, and S.-T. Wu, "High temperature-gradient refractive index liquid crystals," Opt. Express **12**, 2002–2010 (2004).
13. D.-X. Xu, A. Delâge, P. Verly, S. Janz, S. Wang, M. Vachon, P. Ma, J. Lapointe, D. Melati, P. Cheben, and J. H. Schmid, "Empirical model

for the temperature dependence of silicon refractive index from O to C band based on waveguide measurements," Opt. Express **27**, 27229–27241 (2019).
14. Q. Ai, M. Liu, C. Sun, and X. Xia, "Temperature dependence of optical constants for Chinese liquid hydrocarbon fuels in the near-infrared (NIR) region from room temperature to 400 K," Appl. Spectrosc. **71**, 2026–2033 (2017).
15. Y.-F. Chau, T.-J. Yang, and W.-D. Lee, "Coupling technique for efficient interfacing between silica waveguides and planar photonic crystal circuits," Appl. Opt. **43**, 6656–6663 (2004).
16. Y.-F. Chau, H.-H. Yeh, and D. P. Tsai, "Surface plasmon resonances effects on different patterns of solid-silver and silver-shell nanocylindrical pairs," J. Electromagn. Waves Appl. **24**, 1005–1014 (2010).
17. Y.-F. Chau, H.-H. Yeh, and D. P. Tsai, "A new type of optical antenna: plasmonics nanoshell bowtie antenna with dielectric hole," J. Electromagn. Waves Appl. **24**, 1621–1632 (2010).
18. Y.-F. Chau, F.-L. Wu, Z.-H. Jiang, and H.-Y. Li, "Evolution of the complete photonic bandgap of two-dimensional photonic crystal," Opt. Express **19**, 4862–4867 (2011).
19. Y.-F. Chau, C.-Y. Jheng, S.-F. Joe, S.-F. Wang, W. Yang, S.-C. Jheng, Y.-S. Sun, Y. Chu, and J.-H. Wei, "Structurally and materially sensitive hybrid surface plasmon modes in periodic silver-shell nanopearl and its dimer arrays," J. Nanopart. Res. **15**, 1424 (2013).
20. N. T. R. N. Kumara, Y.-F. C. Chau, J.-W. Huang, H. J. Huang, C.-T. Lin, and H.-P. Chiang, "Plasmonic spectrum on 1D and 2D periodic arrays of rod-shape metal nanoparticle pairs with different core patterns for biosensor and solar cell applications," J. Opt. **18**, 115003 (2016).
21. Y.-F. Chou Chau, C.-T. Chou Chao, C. M. Lim, H. J. Huang, and H.-P. Chiang, "Depolying tunable metal-shell/dielectric core nanorod arrays as the virtually perfect absorber in the near-infrared regime," ACS Omega **3**, 7508–7516 (2018).
22. Y.-F. Chou Chau, C.-T. Chou Chao, H. J. Huang, U. Anwar, C. M. Lim, N. Y. Voo, A. H. Mahadi, N. T. R. N. Kumara, and H.-P. Chiang, "Plasmonic perfect absorber based on metal nanorod arrays connected with veins," Results Phys. **15**, 102567 (2019).
23. Y.-F. Chou Chau, C.-T. Chou Chao, H. J. Huang, R. C. Lim, and H.-P. Chiang, "Tunable plasmonic effects arising from metal-dielectric nanorods," Appl. Opt. **58**, 2530–2539 (2019).
24. Y.-F. C. Chau, C.-T. C. Chao, H. J. Huang, Y.-C. Wang, H.-P. Chiang, M. N. Syafi'ie Md Idris, Z. Masri, and C. M. Lim, "Strong and tunable plasmonic field coupling and enhancement generating from the protruded metal nanorods and dielectric cores," Results Phys. **13**, 102290 (2019).
25. Y.-F. C. Chau, "Mid-infrared sensing properties of a plasmonic metal-insulator-metal waveguide with a single stub including defects," J. Phys. D **53**, 115401 (2020).
26. S. Kocaman, R. Chatterjee, N. C. Panoiu, J. F. McMillan, M. B. Yu, R. M. Osgood, D. L. Kwong, and C. W. Wong, "Observation of zeroth-order band gaps in negative-refraction photonic crystal superlattices at near-infrared frequencies," Phys. Rev. Lett. **102**, 203905 (2009).
27. Q. Cheng, R. Liu, D. Huang, T. J. Cui, and D. R. Smith, "Circuit verification of tunneling effect in zero permittivity medium," Appl. Phys. Lett. **91**, 234105 (2007).
28. A. Prain, S. Vezzoli, N. Westerberg, T. Roger, and D. Faccio, "Spontaneous photon production in time-dependent epsilon-near-zero materials," Phys. Rev. Lett. **118**, 133904 (2017).
29. A. M. Mahmoud, I. Liberal, and N. Engheta, "Dipole-dipole interactions mediated by epsilon-and-mu-near-zero waveguide supercoupling," Opt. Express **7**, 415–424 (2017).
30. M. Z. Alam, I. De Leon, and R. W. Boyd, "Large optical nonlinearity of indiumtin oxide in its epsilon-near-zero region," Science **352**, 795–797 (2016).
31. S. B. Cavalcanti, M. de Dios-Leyva, E. Reyes-Gómez, and L. E. Oliveira, "Band structure and band-gap control in photonic superlattices," Phys. Rev. B **74**, 153102 (2006).
32. M. de Dios-Leyva and O. E. González-Vasquez, "Band structure and associated electromagnetic fields in one-dimensional photonic crystals with left-handed materials," Phys. Rev. B **77**, 125102 (2008).
33. M. V. Hobden and J. Warner, "The temperature dependence of the refractive indices of pure lithium niobate," Phys. Lett. **22**, 243–244 (1966).
34. J. Li, "Refractive indices of liquid crystals and their applications in display and photonic devices," Ph.D. dissertation (University of Central Florida, 2005).
35. I. Liberal and N. Engheta, "The rise of near-zero-index technologies," Science **358**, 1540–1541 (2017).